NACA RM L55K23

NACA

RESEARCH MEMORANDUM

THE EFFECTS AT A MACH NUMBER OF 6.86 OF DRAG BRAKES ON THE LIFT, DRAG, AND PITCHING MOMENT OF AN OGIVE CYLINDER

By Jim A. Penland and David E. Fetterman, Jr.

Langley Aeronautical Laboratory
Langley Field, Va.

NATIONAL ADVISORY COMMITTEE FOR AERONAUTICS

WASHINGTON

March 19, 1956

Declassified March 18, 1960

NACA RM L55K23

NATIONAL ADVISORY COMMITTEE FOR AERONAUTICS

RESEARCH MEMORANDUM

THE EFFECTS AT A MACH NUMBER OF 6.86 OF DRAG BRAKES ON THE LIFT, DRAG, AND PITCHING MOMENT OF AN OGIVE CYLINDER

By Jim A. Penland and David E. Fetterman, Jr.

SUMMARY

Results are presented of three-component force tests of a cylindrical body with an ogival nose equipped with panel-type drag brakes each covering approximately 21 percent of the body circumference and located on opposite sides of the body at the rear end. The investigation was made in the Langley 11-inch hypersonic tunnel at a Mach number of 6.86, a Reynolds number of 1.5×10^6 based on body length, angles of attack from -5° to 25°, and brake-deflection angles from 0° to 30°, with the brakes in the vertical and horizontal planes. The comparison of experimental results with the results of Newtonian impact theory shows that the trends of the longitudinal characteristics with angle of attack may be predicted with reasonable accuracy. The drag brakes in the vertical position produce higher total drag and higher negative pitching moments at angles of attack than do the identical brakes in the horizontal position, even though the top drag brake becomes ineffective at high angles of attack.

INTRODUCTION

A hypersonic aircraft or missile flying at extremely high altitudes will encounter aerodynamic heating of increasing intensity as it descends into the atmosphere. This heating may be alleviated by decelerating the aircraft. One means of accomplishing this deceleration is by increasing the total drag of the configuration through the use of drag brakes.

As part of an overall program to investigate an airplane configuration at high supersonic speeds (refs. 1 to 7), an investigation was made to determine the effects on lift, drag, and pitching moment of

panel-type diametrically opposite body flaps located at the rear end of an ogive-cylinder fuselage. These body flaps, or drag brakes, were 1.5 body diameters long and each covered approximately 21 percent of the body circumference. Tests were made in the Langley 11-inch hypersonic tunnel at a Mach number of 6.86 and at a Reynolds number of 1.5×10^6, based on body length. Results are presented for the body alone and the body with drag brakes deflected 10°, 20°, and 30° in both the vertical and horizontal planes. These results are compared with estimates given by the Newtonian impact and shock-expansion theories.

SYMBOLS AND COEFFICIENTS

C_L	lift coefficient, L/qA
C_D	drag coefficient, D/qA
L/D	lift-drag ratio, C_L/C_D
C_m	pitching-moment coefficient, M_Y/qA
$C_{D_{min}}$	minimum drag coefficient, D_{min}/qA
$\Delta C_{D_{min}}$	incremental minimum drag coefficient, $C_{D_{min}} - \left(C_{D_{min}}\right)_{\delta = 0^\circ}$
x_{cp}	center of pressure, percent body length from nose
L	lift force normal to free stream
D	drag force parallel to free stream
M_Y	pitching moment, moment reference 52.67 percent body length from nose
D_{min}	minimum drag, drag at $\alpha = 0^\circ$
q	free-stream dynamic pressure
A	area of base of basic body
l	length of body
M	free-stream Mach number
R	free-stream Reynolds number based on l

δ deflection of drag brake, deg

α angle of attack, deg

MODELS

The drag-brake model configuration used for the present tests consisted of a series of four stainless steel models, the body alone, and the body with 10°, 20°, and 30° drag brakes (fig. 1). The body common to the four models was an ogive nosed circular cylinder and with a fineness ratio of 9.5. The drag brakes consisted of fuselage panels $1\frac{1}{2}$ body diameters long and 0.60 body diameters wide, rotating 10°, 20°, and 30° about their leading edge, and located on the after end of the body. The details and basic dimensions of the models may be seen in figure 2.

STRAIN-GAGE BALANCES

Three external strain-gage balances were used to measure the forces and moments on the models. Two two-component balances of different sensitivities were used to measure both normal and chord force, and a one-component balance of low sensitivity was used to measure pitching moment. Because of this low sensitivity, pitching-moment data were only obtained up to an angle of attack of 15°. Angles of attack were measured from schlieren photographs for all tests. Lift and drag coefficients plotted in the present figures were calculated from the measured normal and chord forces. Base pressures were measured during all tests and the chord-force component was adjusted to correspond to a base pressure equal to stream static pressure. The average adjustment was about 5 percent of the measured chord force.

TESTS

Tests were made at an average stagnation temperature of 675° F to avoid air liquefaction (ref. 8), a stagnation pressure of 20 atmospheres absolute, and a test section Mach number of 6.86. These conditions correspond to a Reynolds number of 1.5×10^6 based on the body length. The absolute humidity was kept to less than 1.87×10^{-5} pounds of water per pound of dry air for all tests. Normal force and chord force were measured at angles of attack from -5° to 25° and pitching moments were measured at angles of attack from -4 to 15°.

PRECISION OF DATA

The maximum uncertainties in the force and moment coefficients for individual test points - due to the balance system and variations in dynamic pressure - have been estimated and are presented as follows:

C_L	± 0.015
C_D	± 0.005
C_m	± 0.005

In general, the faired curves should be more accurate than these values. The angle of attack α was accurate within $\pm 0.1^\circ$.

RESULTS AND DISCUSSION

Drag Brakes in the Horizontal Plane

The longitudinal characteristics, C_L, C_D, L/D, C_m, and x_{cp} are tabulated in tables I and II. The variation with angle of attack of these coefficients is presented in figure 3 for the body alone and the body with drag brakes in the horizontal position at angles of attack up to 25° (C_m and x_{cp} up to only 15°) and drag-brake deflection angles up to 30°. Included for comparison with the experimental data in figure 3 are the longitudinal characteristics as predicted by the Newtonian impact theory (ref. 9).

The predicted aerodynamic characteristics referred to as impact theory were obtained by calculating the characteristics for the ogive nose, the cylindrical afterbody minus the area covered by the drag brakes, and the drag brakes separately using Newtonian impact theory and then adding the various results together to obtain the coefficient for the complete model.

It may be seen that the lift coefficient is predicted with reasonable accuracy with deviations between experiment and theory being greatest for the larger drag-brake deflections and at the higher angles of attack (fig. 3). The shapes of the drag curves are predicted very accurately except at the higher angles of attack for the 20° and 30° drag deflections. The predicted drag values are usually lower than the experimental values probably because the impact theory does not consider skin friction. An exception is the 30° drag-brake model where values of the drag coefficient are slightly overestimated by theory at low angles of attack. This is probably caused by a thickening of the boundary layer ahead of

the drag brake, which may be seen by comparing figure 4(a) with figure 4(g), and the resulting reduction of brake area exposed to the flow. The overestimation of the curves of lift-drag ratio is considerable for all models and follows from the low predicted values of drag and the more reasonable predicted values of lift. The moment coefficients were predicted accurately by the impact theory for the body alone and the 10° brakes (figs. 3(a) and (b). However, for the 20° and 30° brakes in the horizontal plane (figs. 3(c) and 3(d)), the predicted values of pitching-moment coefficient are more negative than the experimental values. This deviation between theory and experiment follows primarily from the higher predicted values of lift coefficient caused by an overestimation of the lift contribution of the horizontal drag brakes and somewhat by the more rearward position of the center of pressure predicted by theory, especially for the 30° brakes in the horizontal plane.

Drag Brakes in the Vertical Plane

The experimental and theoretical longitudinal characteristics of the drag-brake model with the brakes in the vertical position are presented in figure 5. The Newtonian impact theory as applied to the vertical drag-brake models considered the top drag brake as being geometrically shielded from the flow by the body at angles of attack. This shielding has been noted previously and is shown in reference 5 by the decreasing yawing-moment derivative with angle of attack for the "Horizontal tails and top vertical tail configuration." By referring to figure 5 it may be seen that, in general, the results of impact theory adequately predict the experimental variations of C_L, C_D, C_m, and x_{cp} below an angle of attack of 8°. At the higher angles of attack, however, the theoretical predictions deviate considerably from the experimental coefficients. The lift predictions underestimate the measured lift for the brakes in the vertical position thus differing from the case of the brakes in the horizontal position where the lift prediction overestimated the experimental lift for the 20° and 30° brake deflections.

The generally lower predicted values of drag are, as in the case of the horizontal brakes, partially due to the absence of skin friction in the impact theory. The theoretical curves of lift-drag ratio considerably overestimate the experimental lift-drag ratio for the vertical brakes primarily because of these low predicted values of drag. At small angles of attack portions of the 30° vertical brakes are in nonshielded flow and consideration of the aerodynamic forces on these exposed parts results in theoretical lift and drag curves which are nonlinear. Since these trends are not verified by experiment, it may therefore be concluded that the simple geometric shielding used here when considering this blanketing is too approximate to account adequately for the effect of body on the top drag brakes.

Comparison of Drag Brakes

For comparison purposes, the variation of lift, drag, lift-drag ratio, and pitching moment with angle of attack for the various drag-brake model configurations is presented in figures 6 to 9. From figures 6 and 9 it can be seen that the brakes in the vertical position give higher values of lift coefficient and considerably more negative values of the pitching-moment coefficient than do the brakes in the horizontal position. On the other hand, the position of the brakes, whether horizontal or vertical, has little effect on the lift-drag ratio (see fig. 8). By comparing figures 7(a) and 7(b) it is clear that the drag increases with angle of attack at a greater rate for the vertical drag brakes than for the horizontal drag brakes even though the top vertical brake is shielded by the body. The greater rate of drag increase indicated for the vertical brakes occurs for the following reasons:

(1) The flow deflection angles occurring on the lower vertical brake are larger than those on the horizontal brakes for a given angle of attack; and since, at higher Mach numbers, the local pressures increase nonlinearly with flow deflection angle, the local pressures acting on the lower vertical brake increase at a greater rate than those acting on the horizontal brakes.

(2) The boundary layer on the bottom of the fuselage becomes thinner with increasing angle of attack thereby providing, on the lower vertical brake, an increasing effective area which is exposed to the flow.

(3) The lower vertical brake is operating in a region of relatively higher dynamic pressure since it is in the compression region under the body.

A reversal of the preceding trend is observed when comparing the respective drags produced by the horizontal and vertical brakes on the basis of a given lift coefficient (see figs. 6 and 7). In this case a higher drag is obtained from the horizontal brakes because, in order to attain a given lift coefficient, the model with the horizontal brakes must assume a higher angle of attack, and therefore produces a higher drag than the model with the vertical brakes.

The variation of the center of pressure with angle of attack for the various models is presented in figure 10. The addition of the drag brakes to the body tends to reduce the variation of the center of pressure with angle of attack. The models with vertical brakes, in general, give the smaller variation. The values of x_{cp} were obtained through the use of faired normal-force curves. The values of x_{cp} at $\alpha = 0^{\circ}$ was obtained by measuring the slope of the curves of C_m against normal-force coefficient at normal force equal zero.

Minimum Drag

The variation of the incremental minimum drag coefficient with brake-deflection angle is given in figure 11, and it may be seen that a smooth and rapid increase in drag may be obtained by increasing the brake-deflection angle.

Included in figure 11 are the incremental drag coefficients predicted by the use of the impact and shock-expansion theories. The flow over the drag brakes was assumed to be two dimensional for calculation by the shock-expansion method and use was made of the tables and equations presented in reference 10. The results of impact theory give good agreement with experiment throughout the brake-deflection range, slightly underestimating the experimental coefficients at small brake deflections and overestimating at the higher deflections. The shock-expansion theory results, however, considerably overestimate the experimental coefficients throughout the brake-deflection range. This overestimation by theory is probably due to a reduction of the experimental incremental drag caused by the boundary layer buildup along the body. It might be expected that this deviation between theory and experiment would be favorably altered by an increase in Reynolds number.

CONCLUSIONS

Analysis of the experimental data, obtained from tests made in the Langley 11-inch hypersonic tunnel on a cylindrical body of revolution having an ogival nose and equipped with two fuselage panel-type drag brakes at a Mach number of 6.86 and a Reynolds number of 1.5×10^6, leads to the following conclusions:

1. The trends of the longitudinal aerodynamic characteristics with angle of attack and brake-deflection angle may be adequately predicted by the use of the Newtonian impact theory.

2. Although, at high angles of attack, the top vertical brake becomes ineffective because of the blanketing effect or interference of the body on the flow over the top of the model, the drag increases with angle of attack at a greater rate for the drag brakes in the vertical position than in the horizontal position. At a given lift coefficient, however, a larger total drag is obtained with the brakes in the horizontal position.

3. The drag brakes in the vertical position produce considerably larger negative pitching moments than do the brakes in the horizontal position.

4. The total drag of a body of revolution at a Mach number of 6.86 increased over a wide range through the use of fuselage panel-type drag brakes.

Langley Aeronautical Laboratory,
National Advisory Committee for Aeronautics,
Langley Field, Va., November 15, 1955.

REFERENCES

1. Penland, Jim A., Ridyard, Herbert W., and Fetterman, David E. Jr.: Lift, Drag, and Static Longitudinal Stability Data From an Exploratory Investigation at a Mach Number of 6.86 of an Airplane Configuration Having a Wing of Trapezoidal Plan Form. NACA RM L54L03b, 1955.

2. Ridyard, Herbert W., Fetterman, David E., Jr., and Penland, Jim A.: Static Lateral Stability Data From an Exploratory Investigation at a Mach Number of 6.86 of an Airplane Configuration Having a Wing of Trapezoidal Plan Form. NACA RM L55A21a, 1955.

3. Dunning, Robert W., and Ulmann, Edward F.: Static Longitudinal and Lateral Stability Data From An Exploratory Investigation at Mach Number 4.06 of an Airplane Configuration Having a Wing of Trapezoidal Plan Form. NACA RM L55A21, 1955.

4. Dunning, Robert W., and Ulmann, Edward F.: Exploratory Investigation at Mach Number 4.06 of an Airplane Configuration Having a Wing of Trapezoidal Plan Form - Longitudinal and Lateral Control Characteristics. NACA RM L55B28, 1955.

5. Fetterman, David E., Jr., Penland, Jim A., and Ridyard, Herbert W.: Static Longitudinal and Lateral Stability and Control Data From an Exploratory Investigation at a Mach Number of 6.86 of an Airplane Configuration Having a Wing of Trapezoidal Plan Form. NACA RM L55C04, 1955.

6. Dunning, Robert W., and Ulmann, Edward F.: Exploratory Investigation at Mach Number 4.06 of an Airplane Configuration Having a Wing of Trapezoidal Plan Form - Effects of Various Tail Arrangements on the Wing-On and Wing-Off Static Longitudinal and Lateral Stability Characteristics. NACA RM L55D08, 1955.

7. Penland, Jim A., Fetterman, David E. Jr., and Ridyard, Herbert W.: Static Longitudinal and Lateral Stability and Control Characteristics of an Airplane Configuration Having a Wing of Trapezoidal Plan Form With Various Tail Sections and Tail Airfoil Arrangements at a Mach Number of 6.86. NACA RM L55F17, 1955.

8. McLellan, Charles H., and Williams, Thomas W.: Liquefaction of Air in the Langley 11-inch Hypersonic Tunnel. NACA TN 3302, 1954.

9. Grimminger, G., Williams, E. P., and Young, G. B. W.: Lift on Inclined Bodies of Revolution in Hypersonic Flow. Jour. Aero. Sci., vol. 17, no. 11, Nov. 1950, pp. 675-690.

10. Ames Research Staff: Equations, Tables, and Charts for Compressible Flow. NACA Rep. 1135, 1953. (Supersedes NACA TN 1428.)

TABLE I.- AERODYNAMIC CHARACTERISTICS OF THE MODEL AT M = 6.86

(a) Brakes in horizontal plane

α, deg	C_L	C_D	L/D	α, deg	C_L	C_D	L/D
$\delta = 0^\circ$ body alone							
-5.2	-0.305	0.188	-1.63	5.3	0.285	0.186	1.53
-4.3	-.239	.179	-1.33	5.8	.351	.216	1.63
-2.0	-.098	.152	-.64	10.4	.709	.328	2.16
-.2	.000	.143	.00	15.3	1.266	.585	2.16
.3	-.005	.134	-.04	19.8	1.948	1.052	1.85
1.9	.079	.151	.52	24.9	2.708	1.634	1.66
3.9	.200	.177	1.13				
$\delta = 10^\circ$							
-5.3	-0.327	0.217	-1.51	3.8	0.233	0.204	1.14
-4.2	-.251	.203	-1.24	5.3	.346	.220	1.57
-2.3	-.110	.182	-.60	5.7	.393	.241	1.63
-.3	.001	.172	.01	10.3	.809	.368	2.20
.4	.018	.171	.11	15.4	1.410	.658	2.14
1.8	.108	.180	.60	19.9	2.133	1.104	1.93
				24.8	2.988	1.750	1.71
$\delta = 20^\circ$							
-5.1	-0.365	0.323	-1.13	5.3	0.405	0.333	1.22
-4.3	-.282	.311	-.91	5.6	.434	.344	1.26
-2.3	-.130	.303	-.43	10.3	.905	.493	1.84
-.3	.001	.292	.00	15.3	1.568	.829	1.89
.3	.028	.294	.09	20.0	2.182	1.452	1.50
1.7	.114	.303	.38	25.0	3.080	2.200	1.40
3.7	.266	.315	.85				
$\delta = 30^\circ$							
-5.1	-0.366	0.584	-0.63	1.8	0.134	0.564	0.24
-4.3	-.279	.576	-.49	2.4	.140	.570	.25
-2.4	-.117	.570	-.21	3.6	.288	.577	.50
-1.4	-.115	.557	-.21	5.3	.382	.582	.66
-.5	-.044	.554	-.08	5.7	.465	.599	.78
-.4	.014	.554	.02	10.5	.919	.763	1.20
.3	-.002	.542	.00	15.6	1.596	1.156	1.38
.5	.019	.543	.04	20.0	2.328	1.831	1.27
1.6	.083	.561	.15	24.9	3.223	2.634	1.22

(b) Brakes in vertical plane

α, deg	C_L	C_D	L/D	α, deg	C_L	C_D	L/D
$\delta = 10^\circ$							
-5.4	-0.384	0.223	-1.72	5.5	0.414	0.222	1.86
-4.2	-.305	.200	-1.53	5.8	.438	.246	1.78
-2.4	-.158	.176	-.90	10.3	.896	.392	2.28
-.1	-.010	.173	-.06	15.3	1.543	.719	2.15
.2	.033	.165	.20	19.8	2.241	1.258	1.78
1.8	.137	.175	.78	25.1	3.022	1.929	1.57
3.6	.279	.203	1.38				
$\delta = 20^\circ$							
-5.2	-0.518	0.338	-1.53	5.3	0.555	0.342	1.62
-4.2	-.418	.314	-1.33	5.7	.643	.372	1.73
-2.3	-.215	.293	-.73	10.3	1.147	.598	1.92
-.4	.017	.308	.05	14.6	1.742	.992	1.76
.1	.024	.301	.08	19.8	2.468	1.580	1.56
1.6	.257	.296	.87	24.7	3.216	2.264	1.42
3.8	.450	.313	1.44				
$\delta = 30^\circ$							
-5.3	-0.734	0.612	-1.20	5.3	0.733	0.606	1.21
-4.3	-.596	.577	-1.03	5.5	.811	.627	1.29
-2.5	-.296	.563	-.53	10.6	1.444	.993	1.45
-.4	-.035	.566	-.06	15.3	2.176	1.511	1.44
.5	-.014	.553	-.03	20.0	2.733	2.176	1.26
1.8	.211	.558	.38	24.8	3.378	2.894	1.17

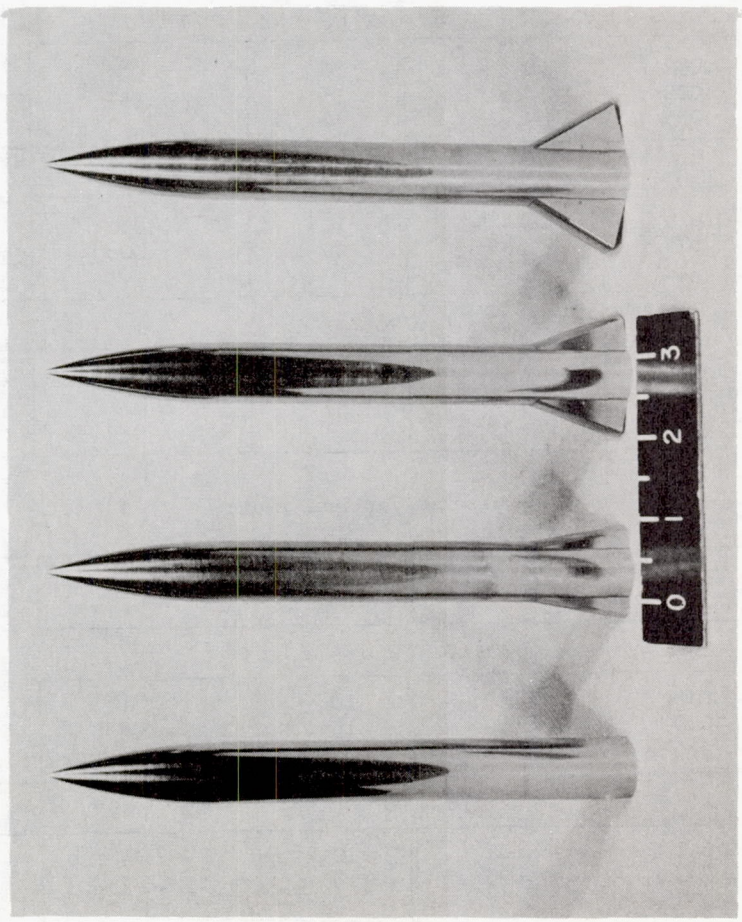
TABLE II.- AERODYNAMIC CHARACTERISTICS OF THE MODEL AT M = 6.86

(a) Brakes in horizontal plane

α, deg	C_m	x_{cp}	α, deg	C_m	x_{cp}
$\delta = 0^\circ$ body alone					
-4	-0.052	0.333	10	0.085	0.418
0	.012	.330	15	.108	.448
5	.055	.329			
$\delta = 30^\circ$					
-4	-0.032	0.394	10	0.047	0.472
0	.002	.415	15	.041	.500
5	.035	.435			
$\delta = 10^\circ$					
-4	-0.018	0.474	10	0.010	0.538
0	-.003	.493	15	.008	.522
5	.012	.493			
$\delta = 20^\circ$					
-4	-0.003	0.519	10	-0.028	0.556
0	.000	.530	15	-.093	.578
5	-.001	.530			

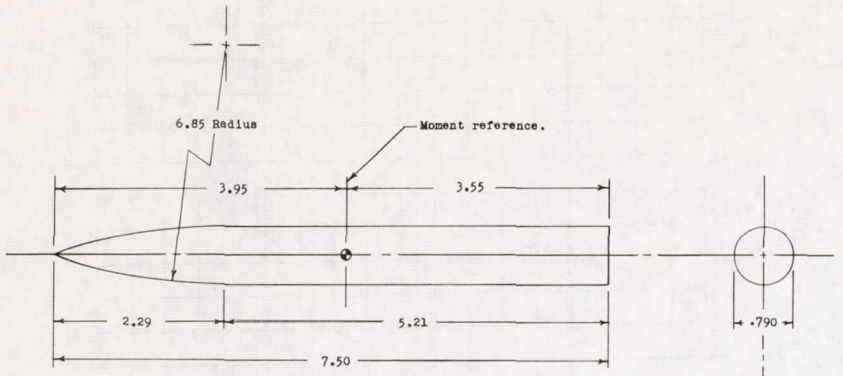
(b) Brakes in vertical plane

α, deg	C_m	x_{cp}	α, deg	C_m	x_{cp}
$\delta = 10^\circ$					
-4	-0.018	0.467	10	0.016	0.510
0	.000	.480	15	-.005	.530
5	.015	.490			
$\delta = 20^\circ$					
-4	0.041	0.602	10	-0.114	0.628
0	.000	.625	15	-.207	.629
5	-.055	.647			
$\delta = 30^\circ$					
-4	0.108	0.719	10	-0.268	0.698
0	-.003	.715	15	-.355	.673
5	-.140	.704			

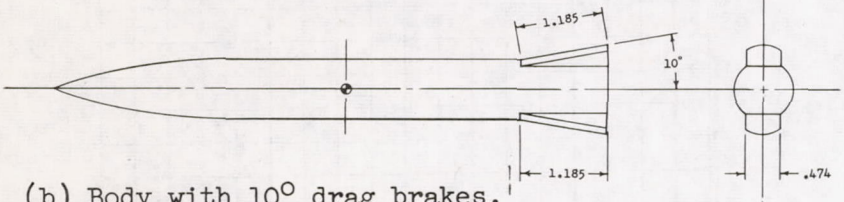


L-88035

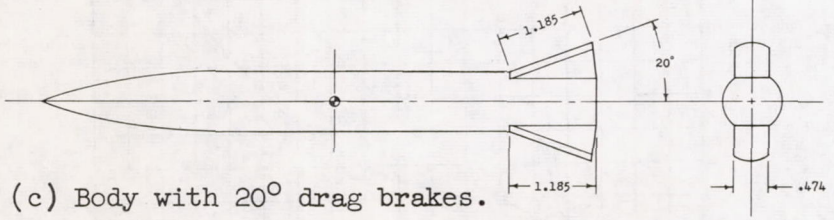
Figure 1.- Photograph of drag brake models.



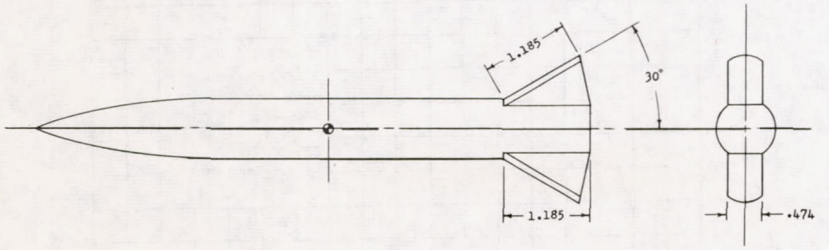
(a) Body alone.



(b) Body with 10° drag brakes.

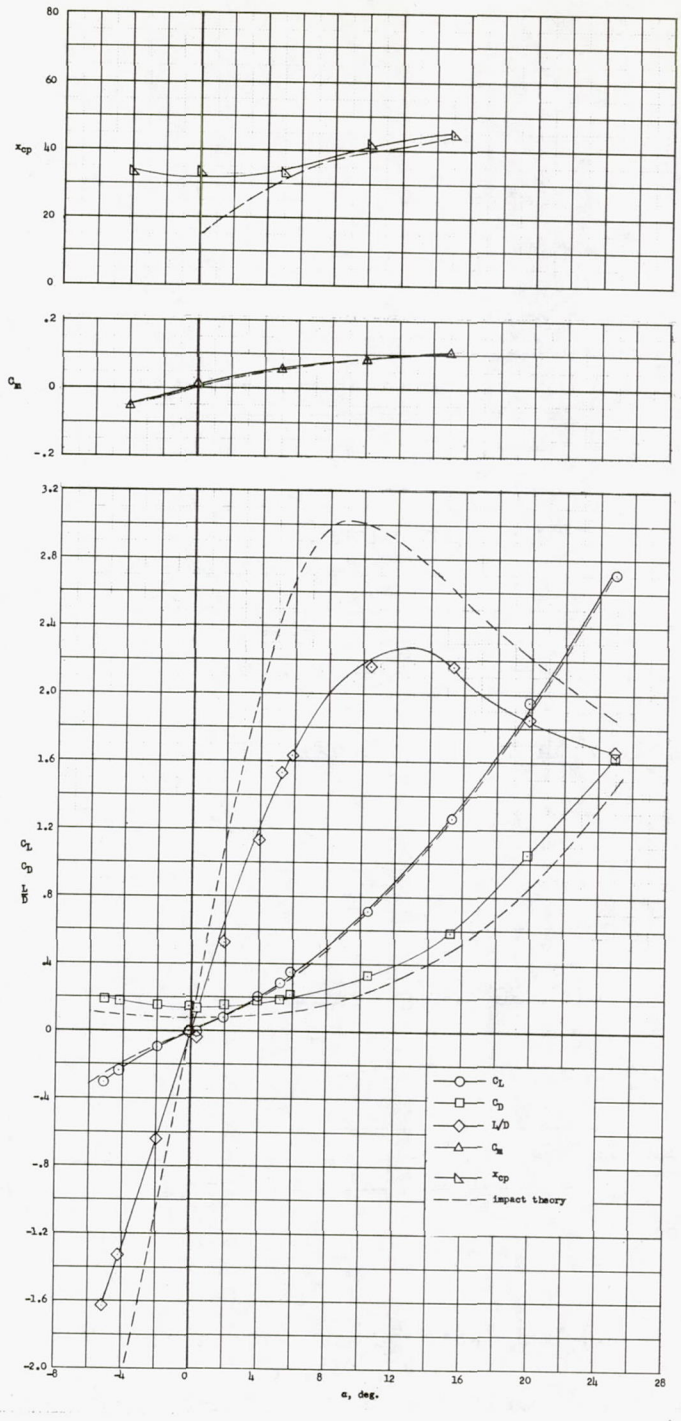


(c) Body with 20° drag brakes.



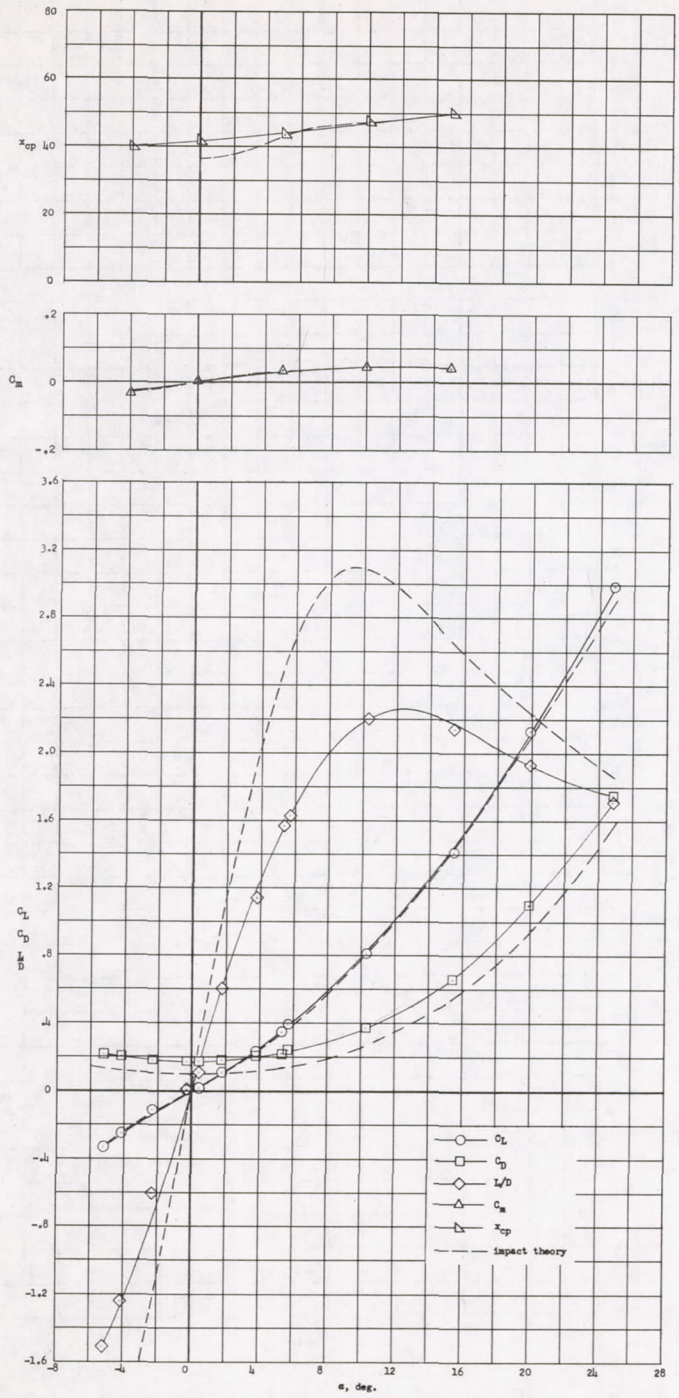
(d) Body with 30° drag brakes.

Figure 2.- Details and basic dimensions of drag brake models. All dimensions are in inches.



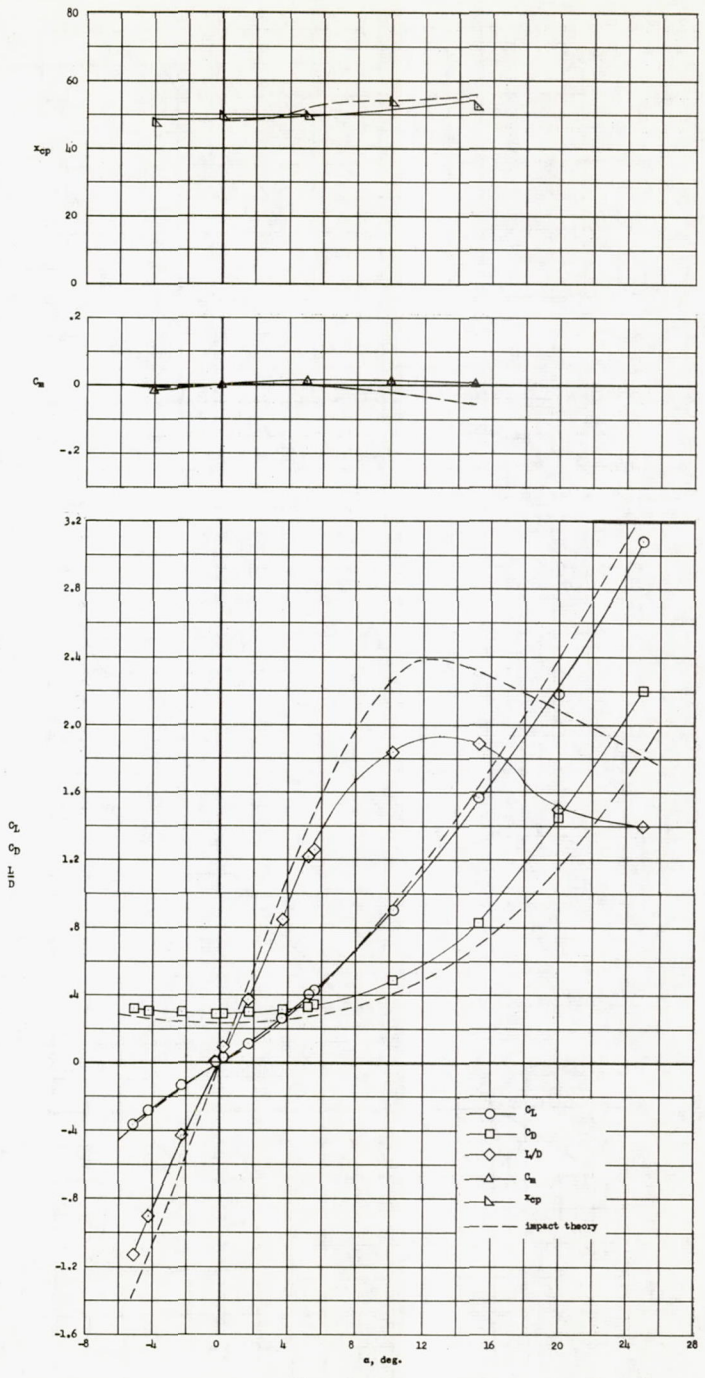
(a) $\delta = 0^{\circ}$; body alone.

Figure 3.- Variation of the longitudinal characteristics of the drag brake models with angle of attack for various drag brake deflections with the brakes in horizontal positions. $M = 6.86$; $R = 1.5 \times 10^6$.



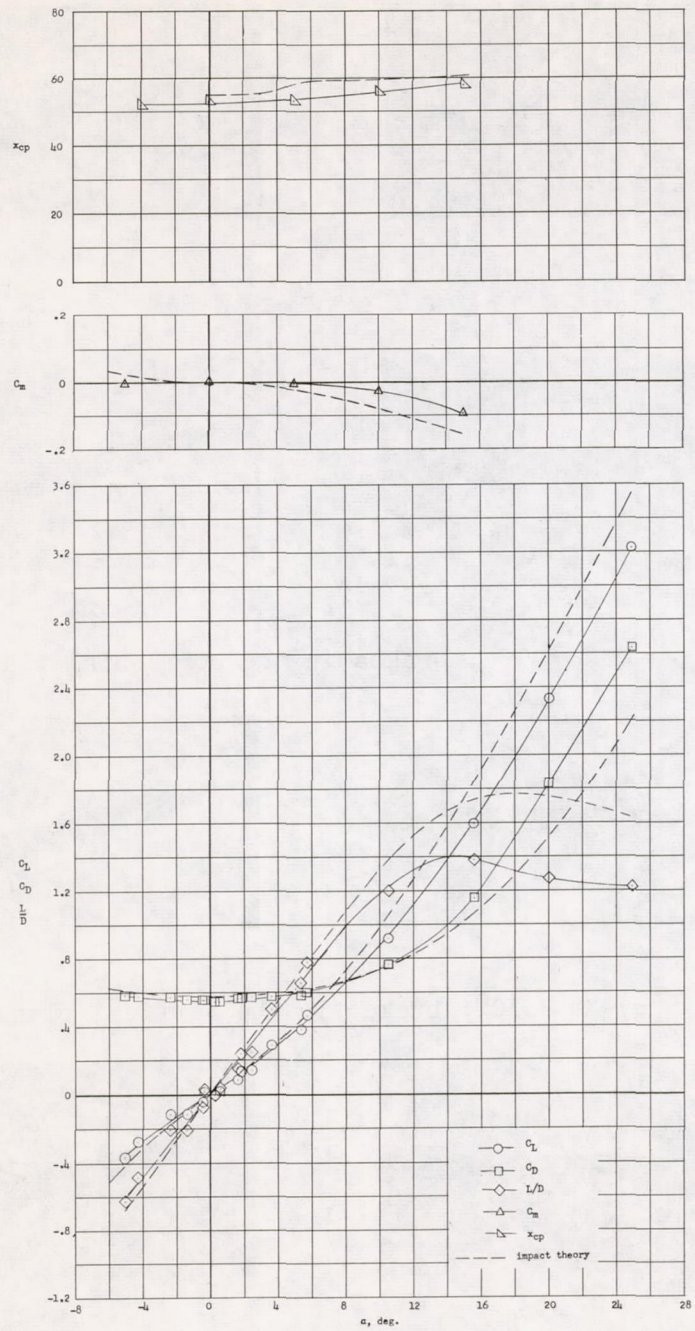
(b) $\delta = 10^{\circ}$; brakes in the horizontal plane.

Figure 3.- Continued.



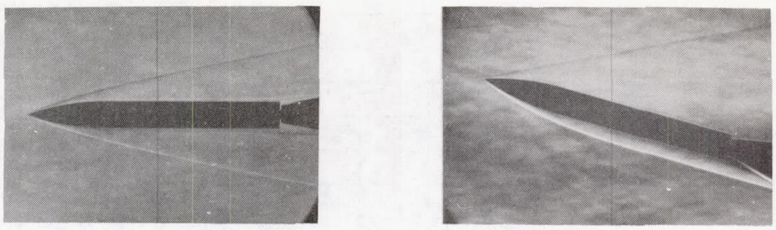
(c) $\delta = 20^{\circ}$; brakes in the horizontal plane.

Figure 3.- Continued.



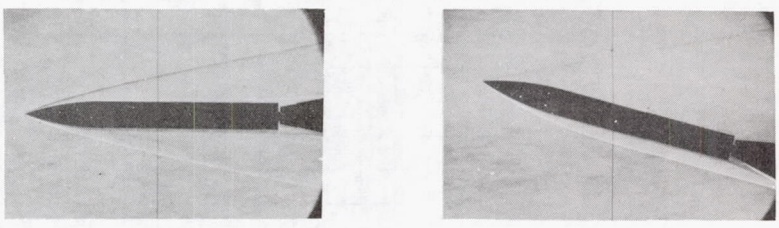
(d) $\delta = 30^{\circ}$; brakes in the horizontal plane.

Figure 3.- Concluded.



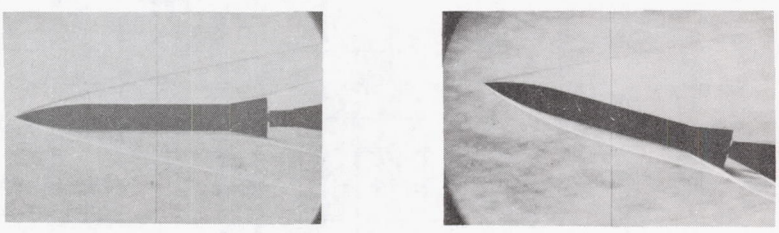
α = 0.3 α = 15.3

(a) $\delta = 0^{\circ}$; body alone.



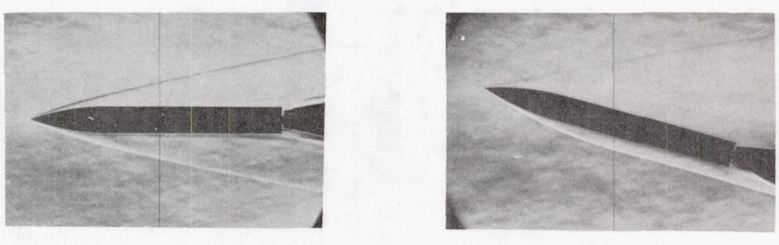
α = 0.4 α = 15.4

(b) $\delta = 10^{\circ}$; brakes in the horizontal plane.



α = -0.2 α = 15.3

(c) $\delta = 10^{\circ}$; brakes in the vertical plane.

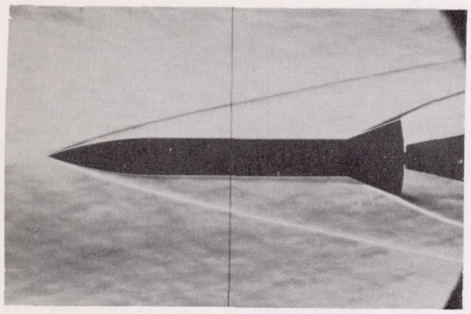


α = 0.3 α = 15.3

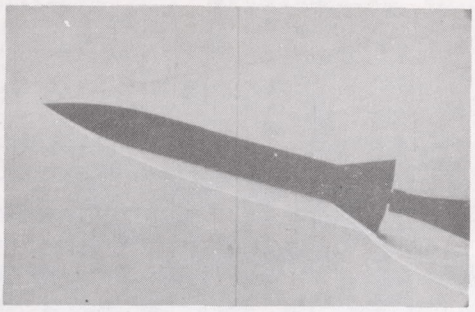
(d) $\delta = 20^{\circ}$; brakes in the horizontal plane.

L-91674

Figure 4.- Typical schlieren photographs of drag brake models in the horizontal and vertical positions at $\alpha = 0^{\circ}$ and 15°. M = 6.86; R = 1.5×10^{6}.

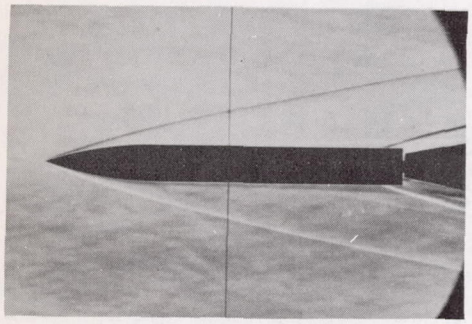


α = 0.1

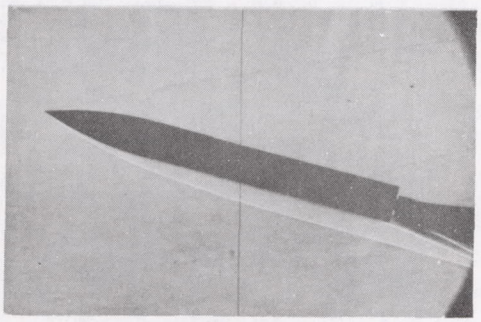


α = 14.5

(e) $\delta = 20^{\circ}$; brakes in the vertical plane.

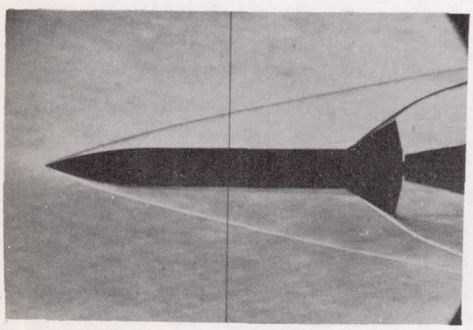


α = 0.5

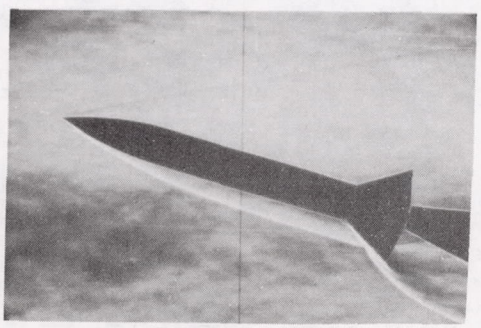


α = 14.8

(f) $\delta = 30^{\circ}$; brakes in the horizontal plane.



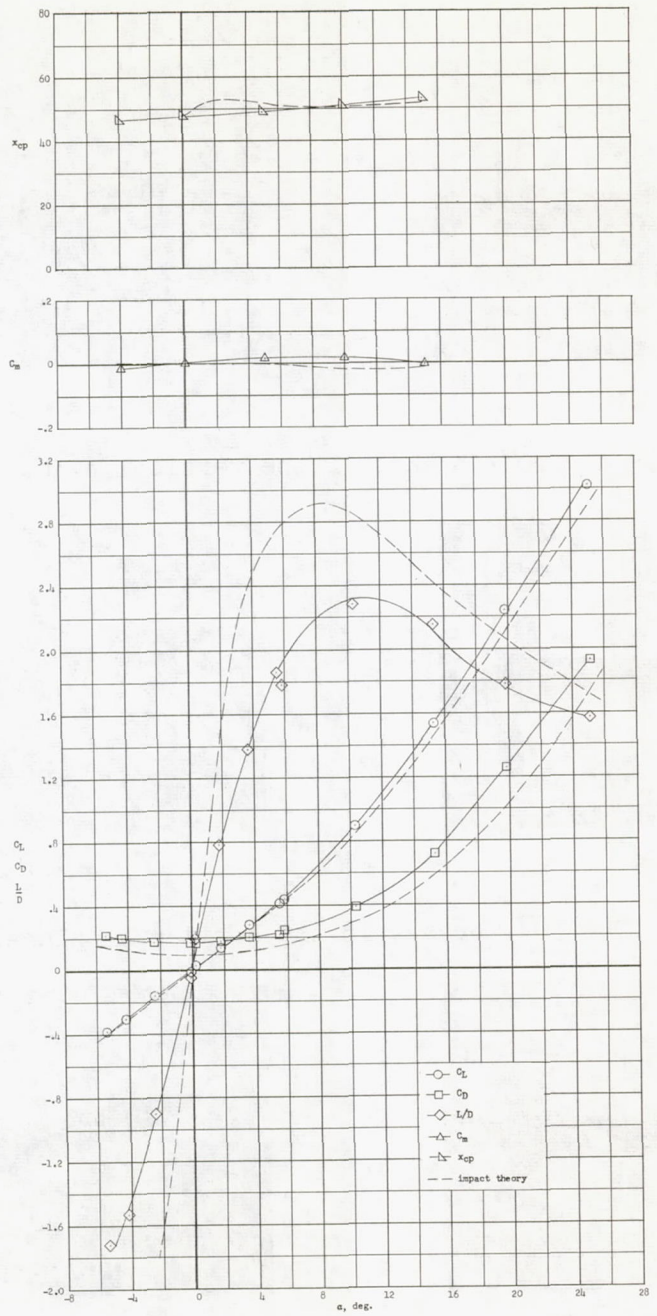
α = 0.5



α = 15.3

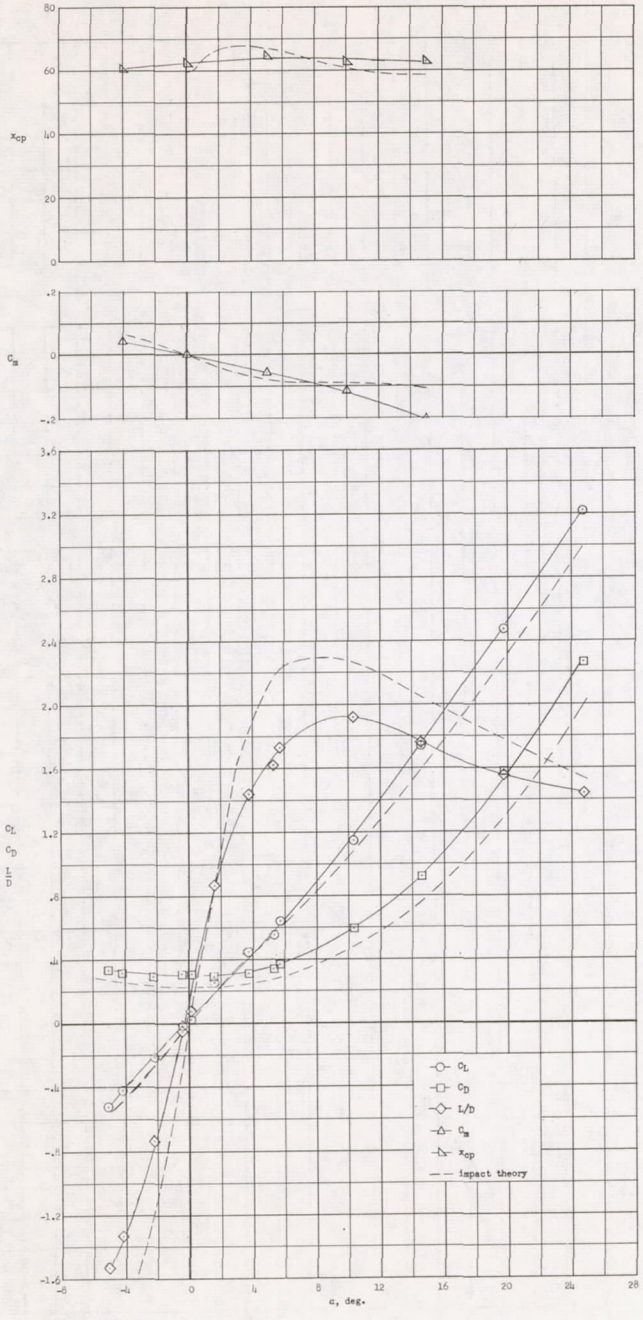
(g) $\delta = 30^{\circ}$; brakes in the vertical plane. L-91675

Figure 4.- Concluded.



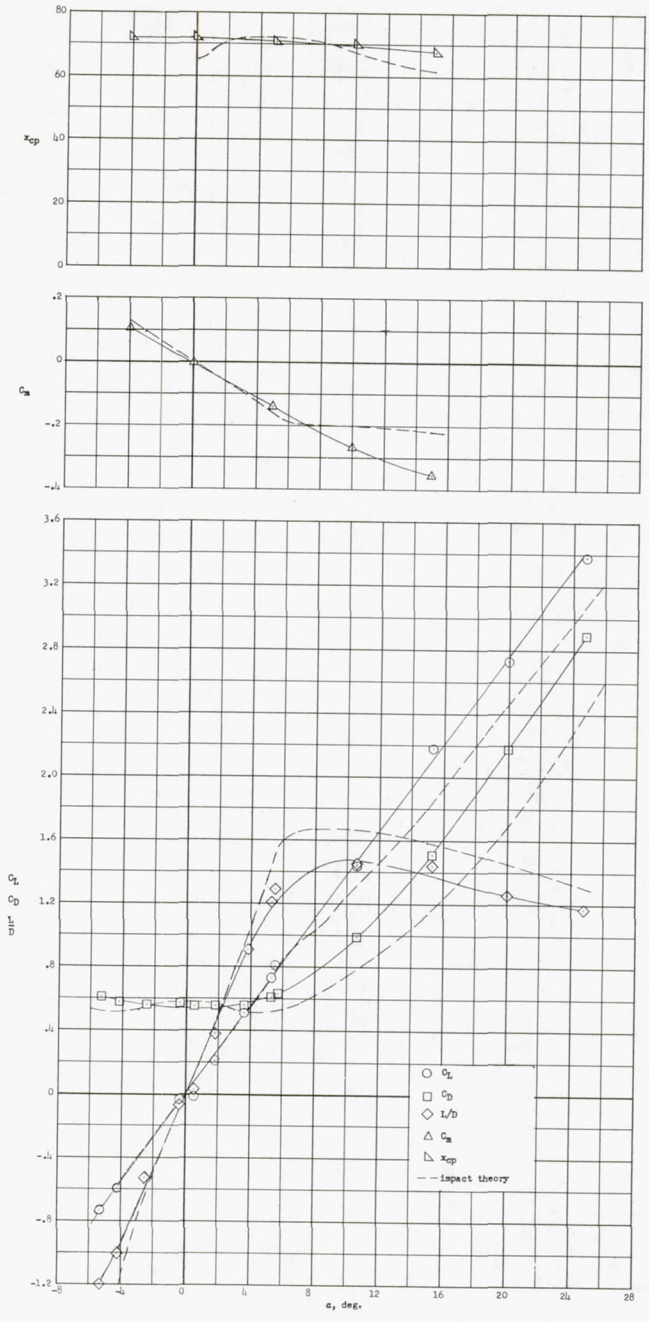
(a) $\delta = 10^{\circ}$; brakes in the vertical plane.

Figure 5.- Variation of the longitudinal characteristics of the drag brake models with angle of attack for various drag brake deflections with the brakes in vertical positions. M = 6.86; R = 1.5×10^6.



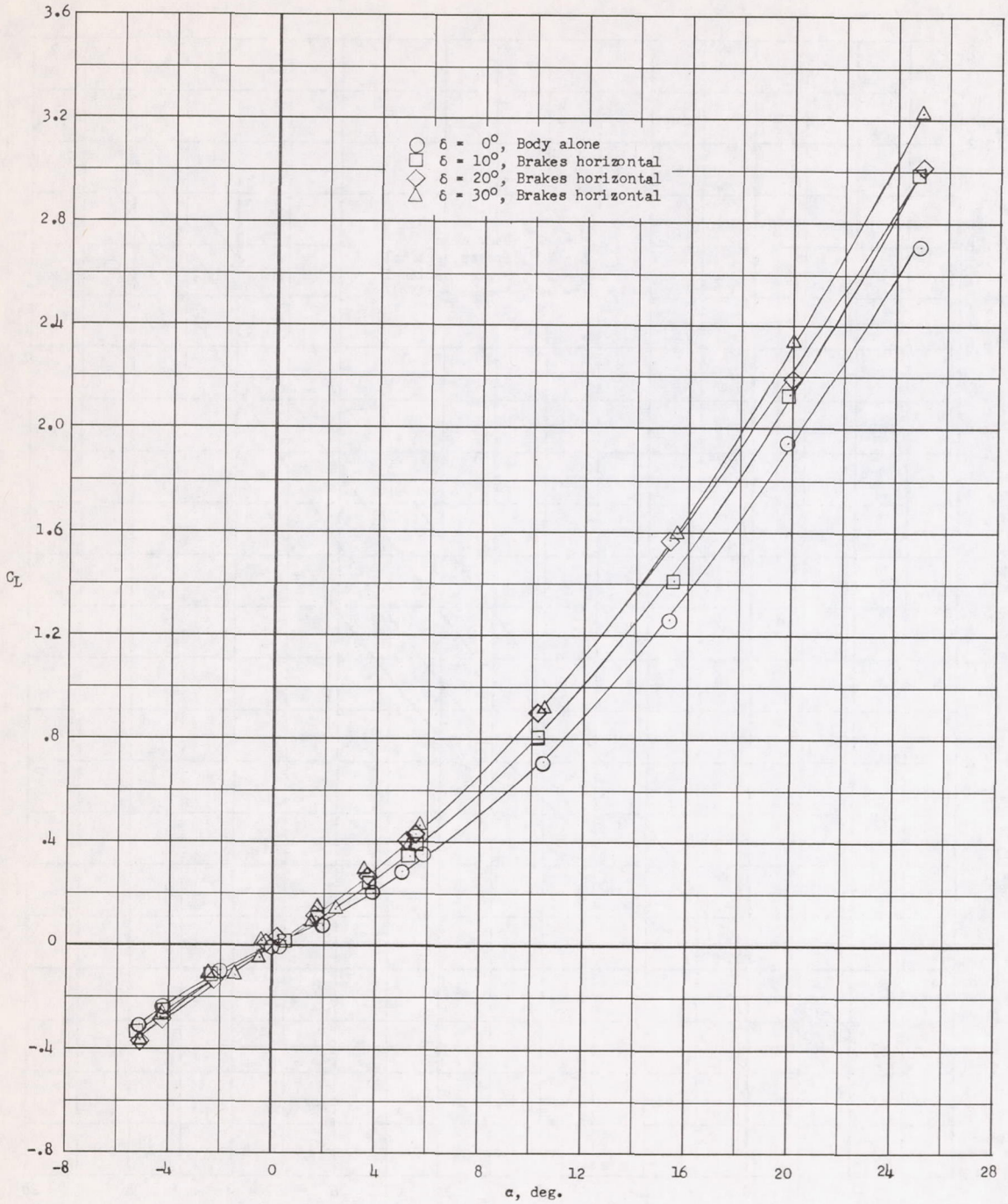
(b) $\delta = 20^{\circ}$; brakes in the vertical plane.

Figure 5.- Continued.



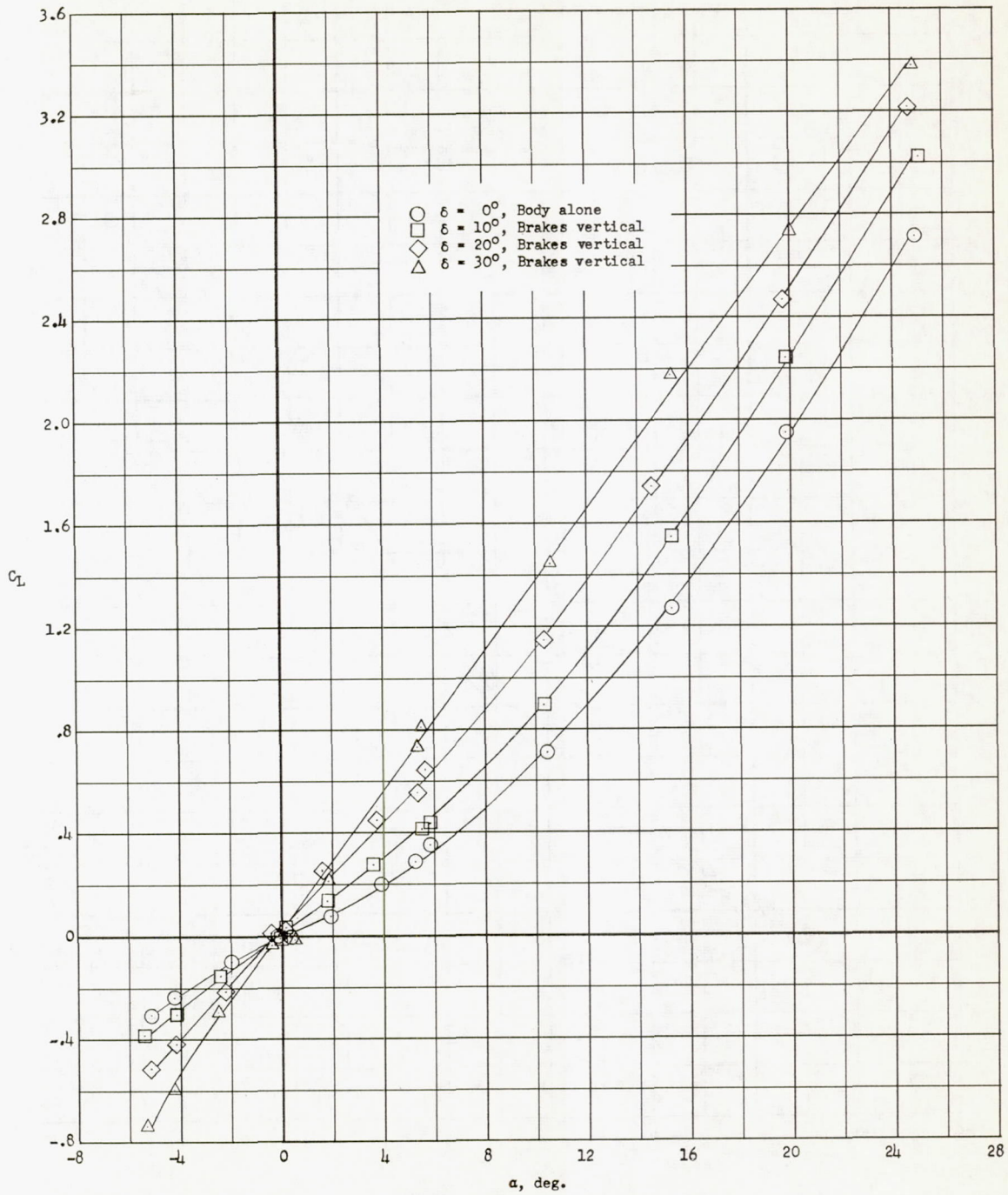
(c) $\delta = 30^{\circ}$; brakes in the vertical plane.

Figure 5.- Concluded.



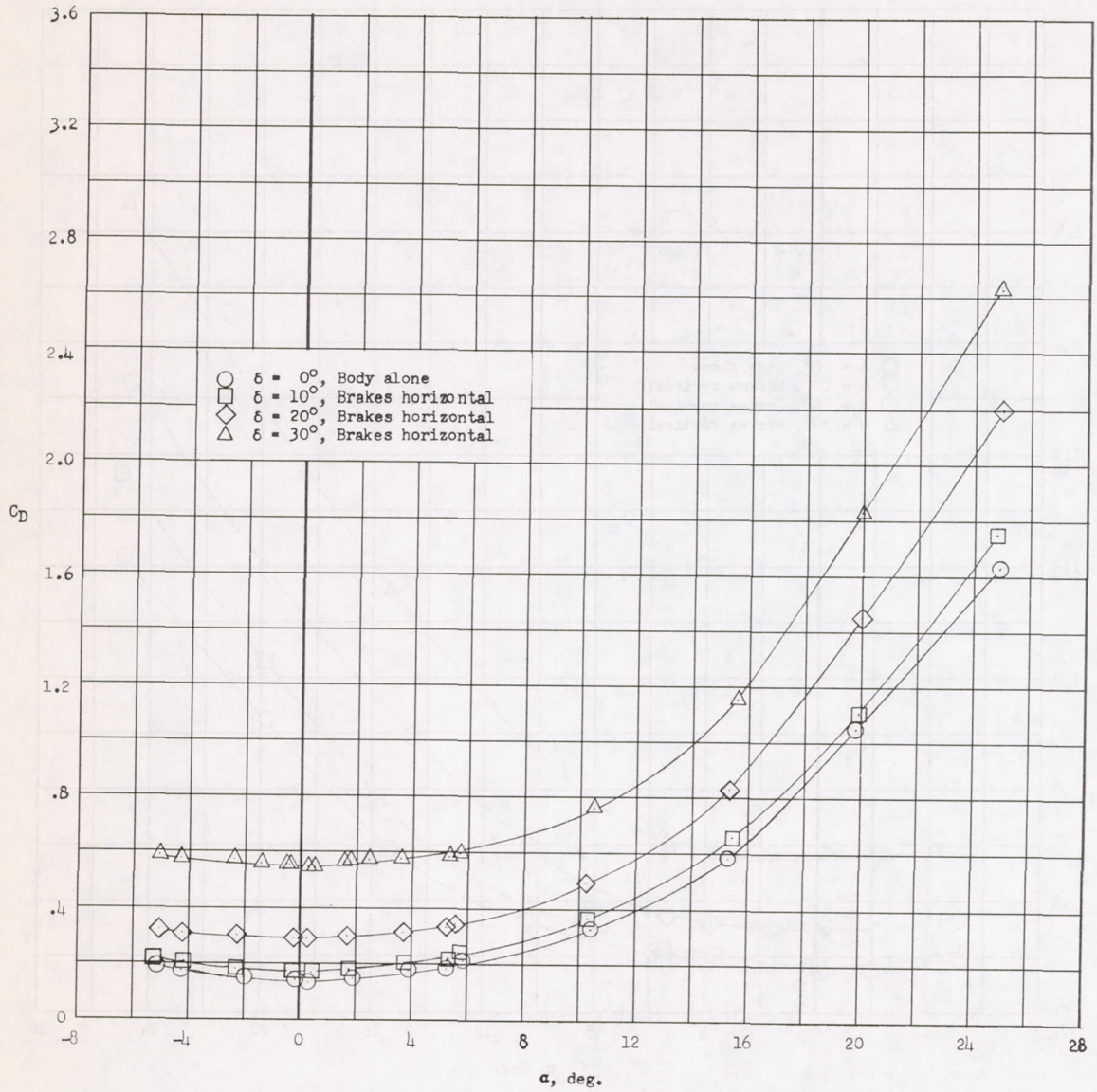
(a) Brakes in the horizontal plane.

Figure 6.- Variation of lift coefficient with angle of attack for various drag brake model configurations. M = 6.86; R = 1.5×10^6.



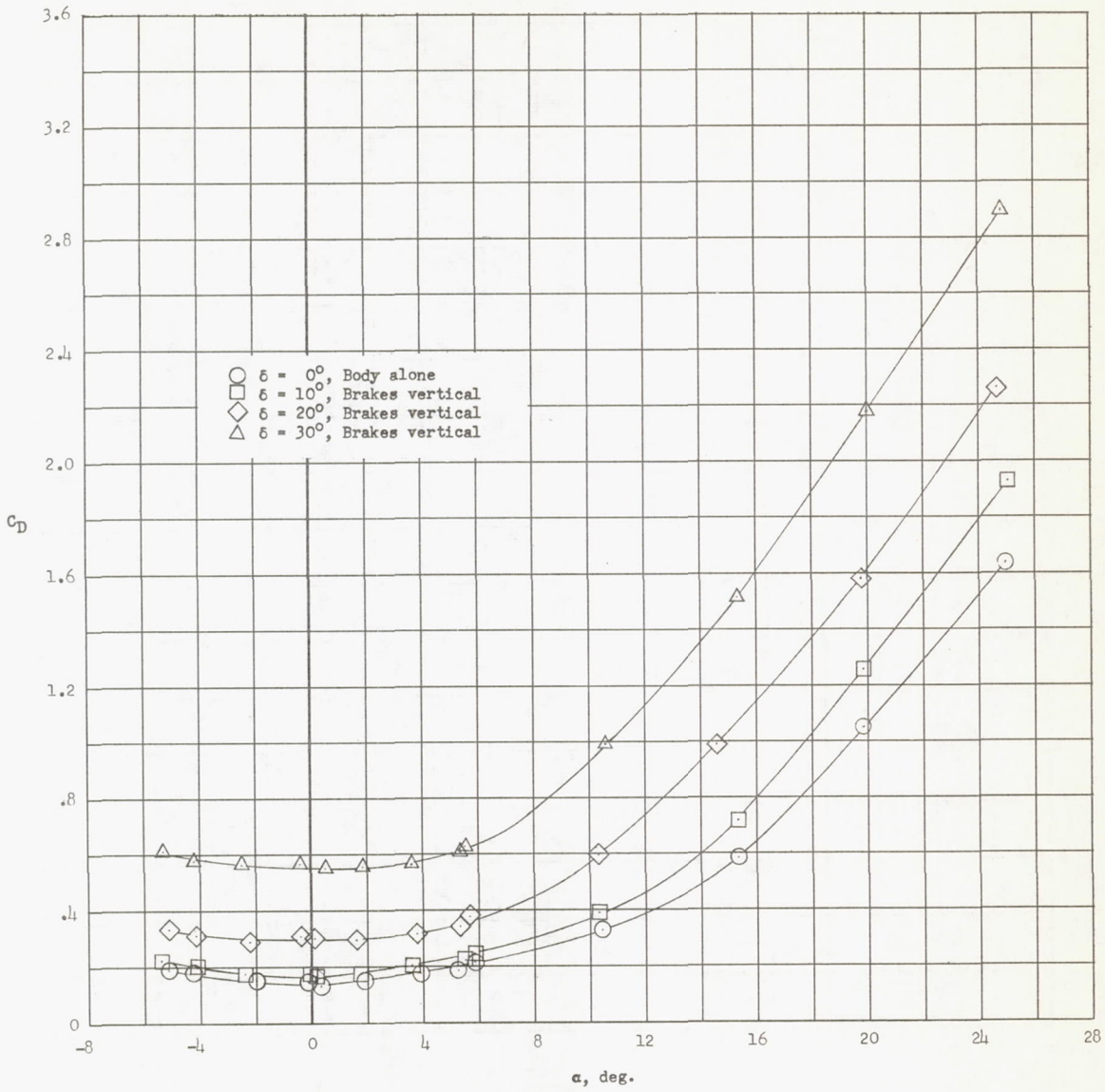
(b) Brakes in the vertical plane.

Figure 6.- Concluded.



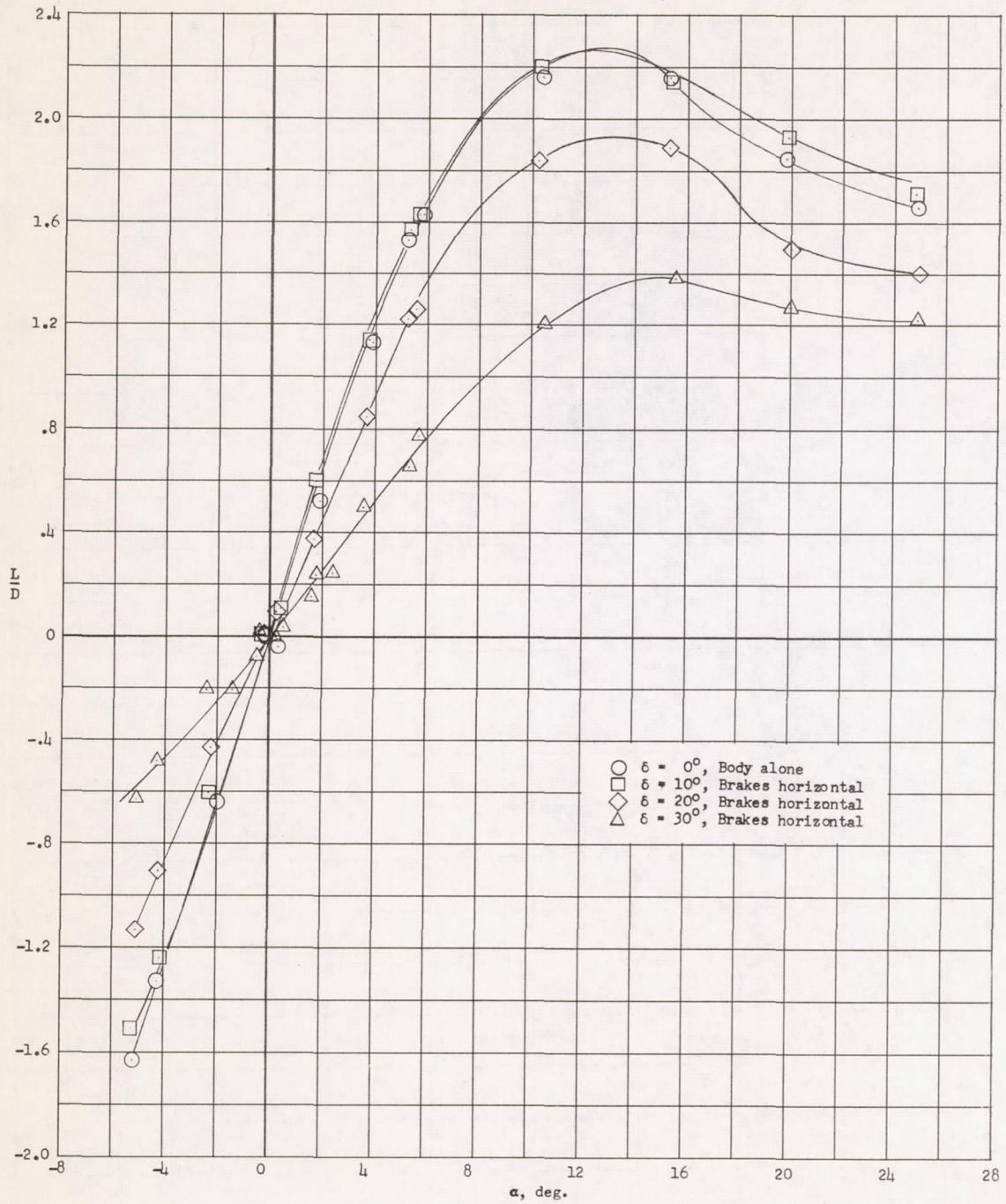
(a) Brakes in the horizontal plane.

Figure 7.- Variation of drag coefficient with angle of attack for various drag brake model configurations. M = 6.86; R = 1.5×10^6.



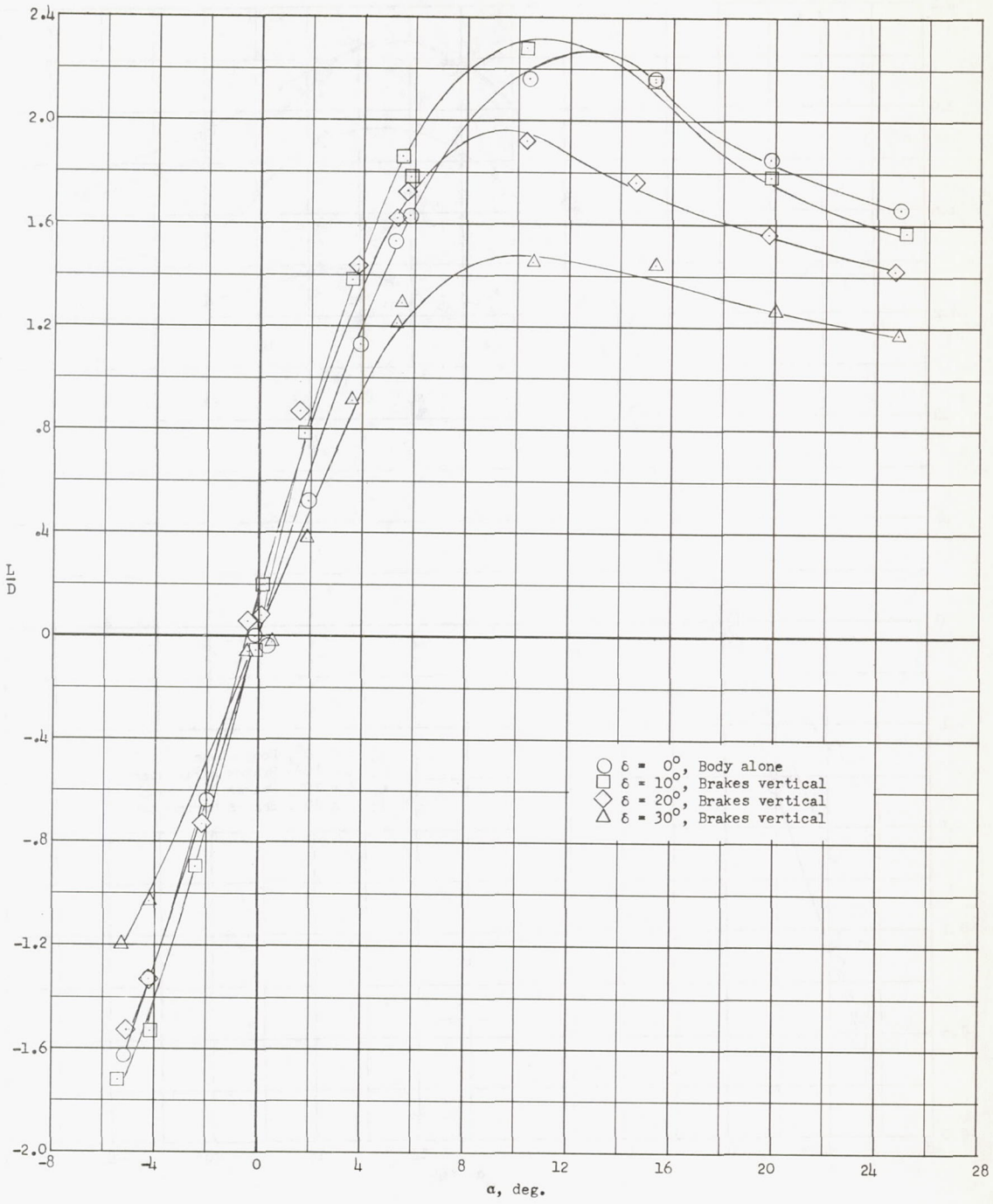
(b) Brakes in the vertical plane.

Figure 7.- Concluded.



(a) Brakes in the horizontal plane.

Figure 8.- Variation of lift-drag ratio with angle of attack for various drag brake model configurations. M = 6.86; R = 1.5×10^6.



(b) Brakes in the vertical plane.

Figure 8.- Concluded.

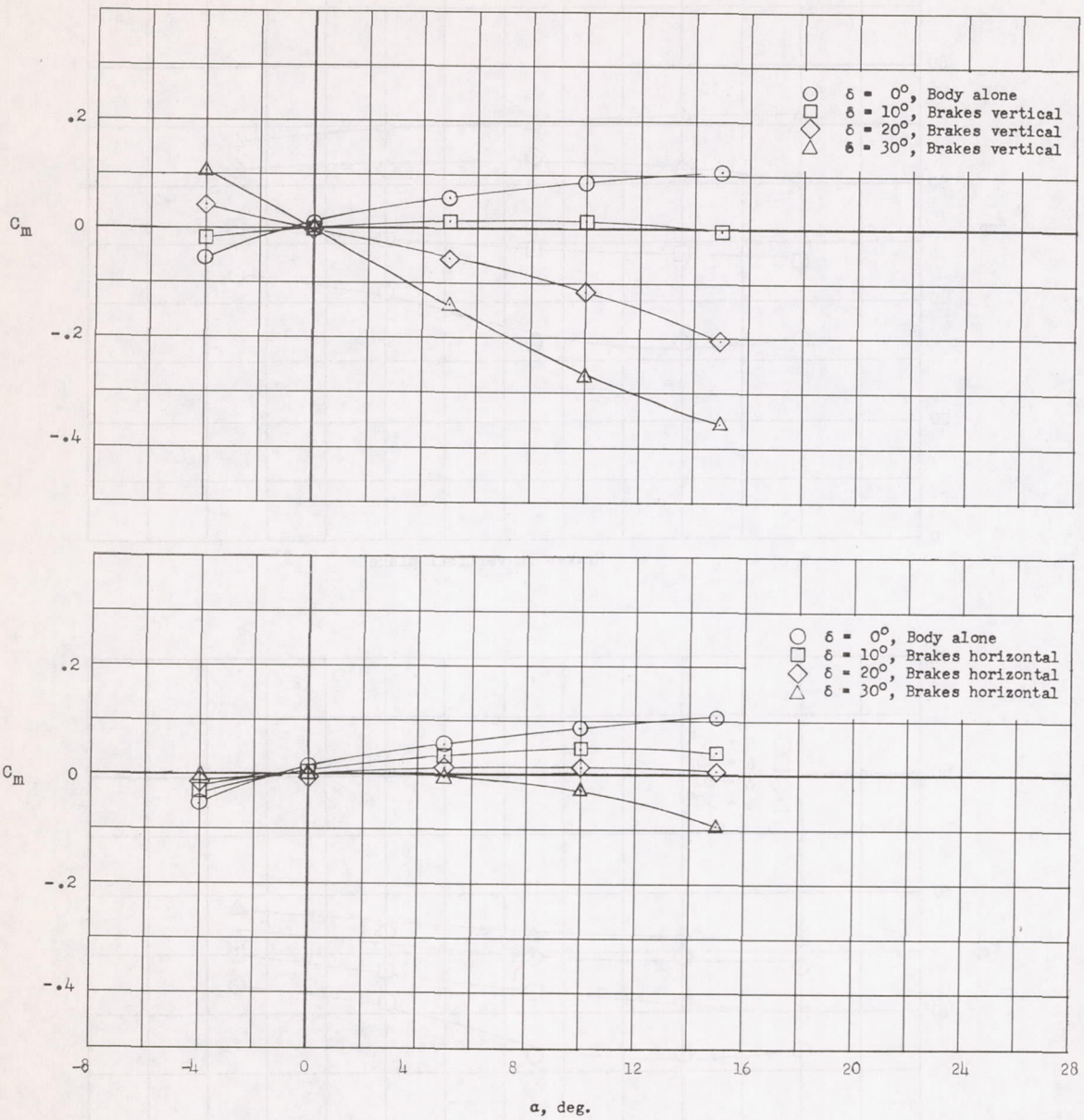


Figure 9.- Variation of pitching-moment coefficient with angle of attack for various drag brake model configurations. M = 6.86; R = 1.5×10^6.

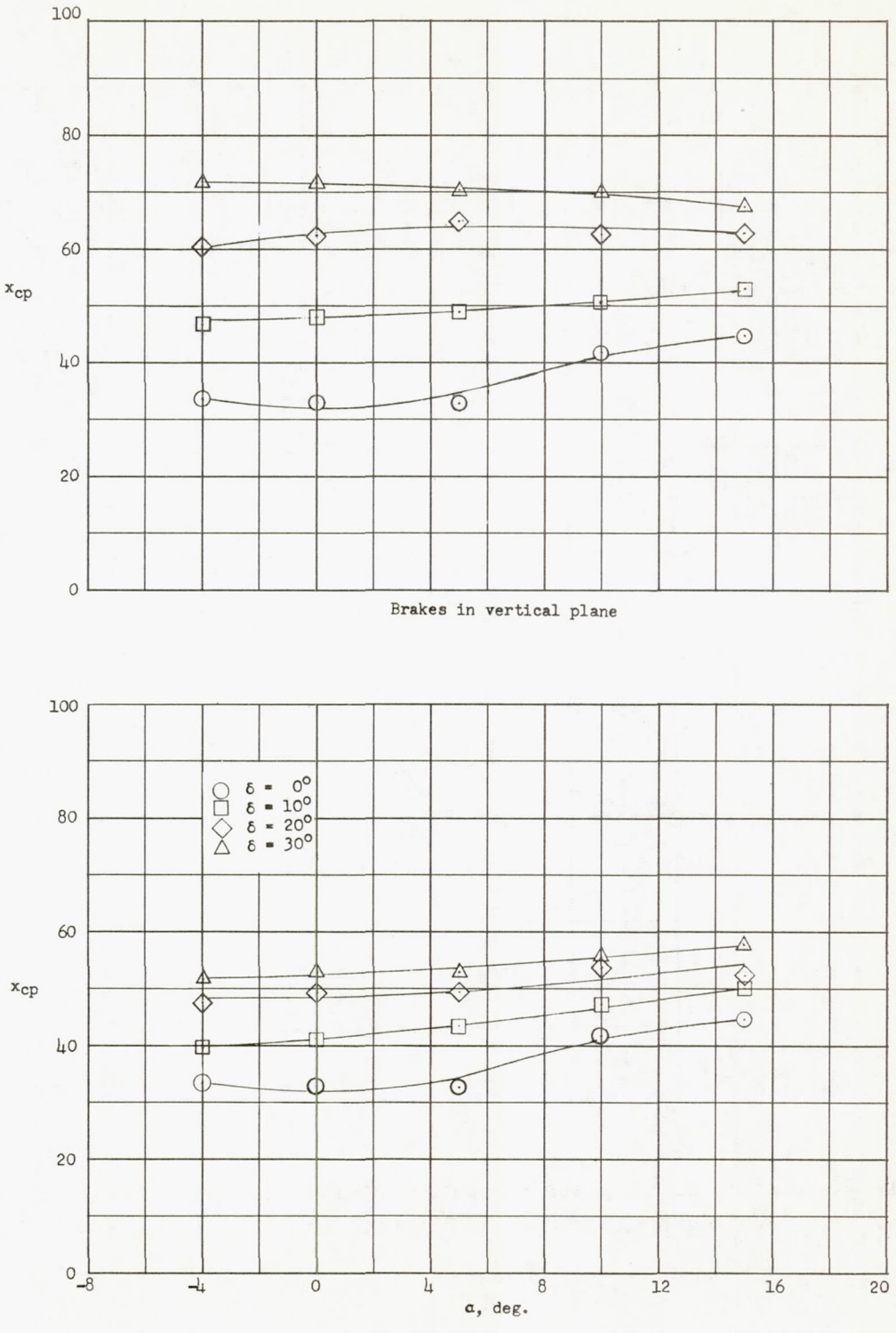


Figure 10.- Variation of center of pressure with angle of attack for various drag brake model configurations. M = 6.86; R = 1.5×10^6.

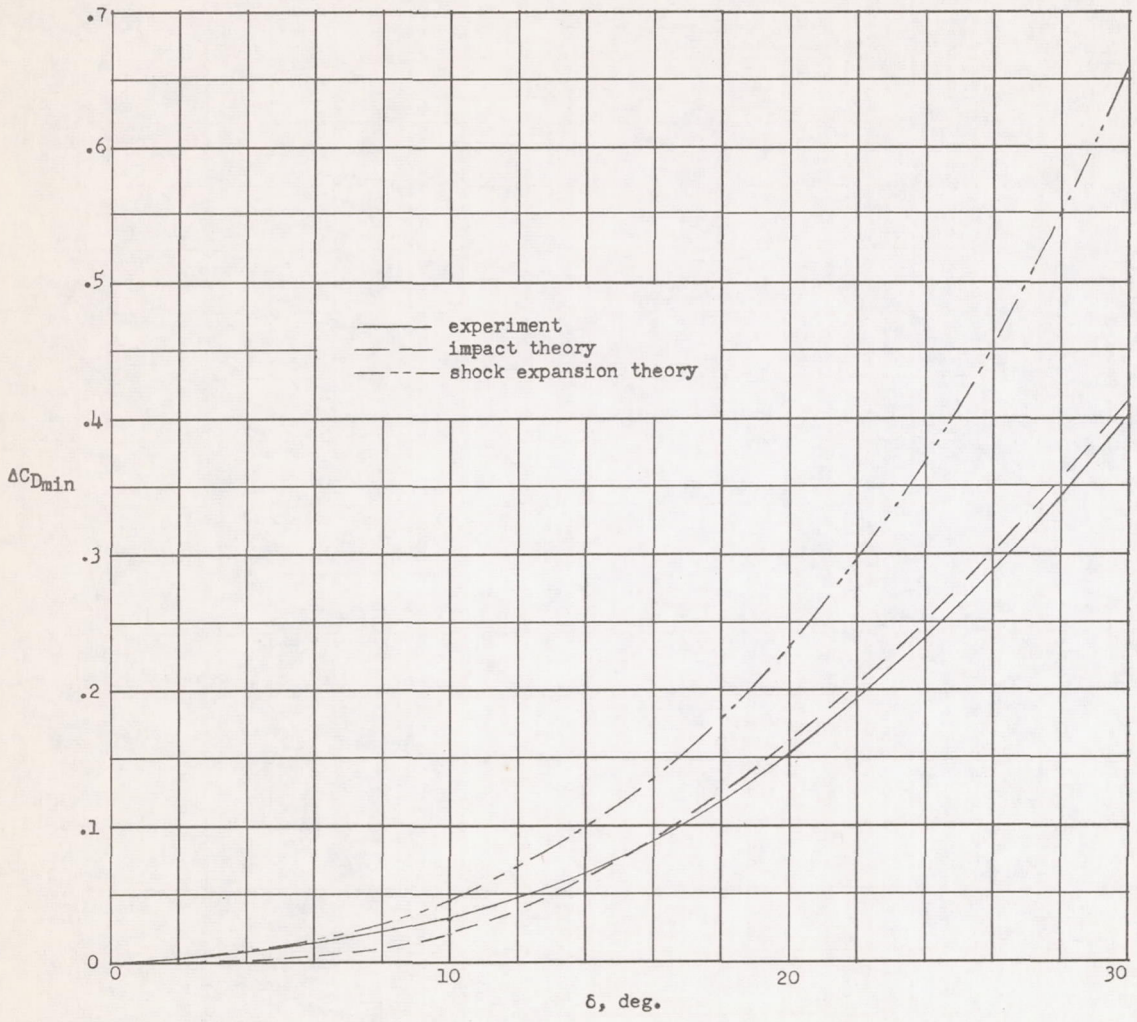


Figure 11.- Variation of incremental minimum drag coefficient with drag brake deflection angle. M = 6.86; R = 1.5×10^6.